Hindawi
Journal of Nanomaterials
Volume 2021, Article ID 5571663, 11 pages
https://doi.org/10.1155/2021/5571663

Research Article

Silver and Gold Nanoparticles from *Limnophila rugosa* Leaves: Biosynthesis, Characterization, and Catalytic Activity in Reduction of Nitrophenols

Van Thuan Le,[1,2] **Ngoc Nhu Quynh Ngu**,[3] **Tan Phat Chau**,[4] **Thi Dung Nguyen**,[5] **Van Toan Nguyen**,[5] **Thi Lan Huong Nguyen**,[6] **Xuan Thang Cao**,[3] **and Van-Dat Doan**[3]

[1]*Center for Advanced Chemistry, Institute of Research and Development, Duy Tan University, 03 Quang Trung, Da Nang 550000, Vietnam*
[2]*The Faculty of Environmental and Chemical Engineering, Duy Tan University, 03 Quang Trung, Da Nang 550000, Vietnam*
[3]*Faculty of Chemical Engineering, Industrial University of Ho Chi Minh City, 12 Nguyen Van Bao, Ho Chi Minh 700000, Vietnam*
[4]*Institute of Applied Science & Technology, Van Lang University, Ho Chi Minh 700000, Vietnam*
[5]*Division of Food Biotechnology, Biotechnology Center of Ho Chi Minh City, Ho Chi Minh City 700000, Vietnam*
[6]*Institute of Biotechnology and Food Technology, Industrial University of Ho Chi Minh City, Ho Chi Minh 700000, Vietnam*

Correspondence should be addressed to Van-Dat Doan; doanvandat@iuh.edu.vn

Received 6 January 2021; Accepted 3 May 2021; Published 21 May 2021

Academic Editor: Hassan Karimi-Maleh

Copyright © 2021 Van Thuan Le et al. This is an open access article distributed under the Creative Commons Attribution License, which permits unrestricted use, distribution, and reproduction in any medium, provided the original work is properly cited.

This study describes a simple green method for the synthesis of *Limnophila rugosa* leaf-extract-capped silver and gold nanoparticles without using any expensive toxic reductant or stabilizer. The noble metal nanoparticles were characterized by Fourier transform infrared (FTIR) microscopy, powder X-ray diffraction (XRD), field emission scanning electron microscopy (FE-SEM), energy-dispersive X-ray analysis (EDX), high-resolution transmission electron microscopy (HR-TEM), selected area electron diffraction (SAED), and dynamic light scattering (DLS) method. It has been found that the biosynthesized silver and gold nanoparticles are nearly spherical in shape with a mean particle size distribution of 87.5 nm and 122.8 nm, respectively. XRD and SAED patterns confirmed the crystalline nanostructure of the metal nanoparticles. FTIR spectra revealed the functional groups of biomolecules presented in the extract possibly responsible for reducing metallic ions and stabilizing formed nanoparticles. The biosynthesized metal nanoparticles have potential application in catalysis. Compared to previous reports, *Limnophila rugosa* leaf-extract-capped silver and gold nanoparticles exhibited a good catalytic activity in the reduction of several derivatives of nitrophenols including 1,4-dinitrobenzene, 2-nitrophenol, 3-nitrophenol, and 4-nitrophenol.

1. Introduction

In the past two decades, noble metal nanoparticles (MNPs), especially silver (AgNPs) and gold nanoparticles (AuNPs), have increasingly attained great attention from the scientific community as well as society due to their distinctive biological, physical, chemical, and optical properties [1, 2]. They have found many applications in diverse areas, such as electronics [3], biotechnology [4, 5], beauty care products [6], drug delivery [7, 8], biosensing, and catalysis [9, 10]. During the last decade, many physical, chemical, and biological synthesis methods focusing on the control of the size and shape of MNPs have been explored [11–13]. Among the approaches mentioned above, biogenic/green synthesis of MNPs using plant extracts received special attention because of it being low cost and environmentally benign without using any expensive and toxic reducing agents as well as stabilizing agents [14, 15]. The first report about using a plant extract for the synthesis of noble MNPs was recognized in 2003 when Gardea-Torresdey et al. showed the effectiveness of *Alfalfa sprouts* extract in the formation of AgNPs under normal conditions within a short time [16]. Since then, extracts from many plants such as *Salvia officinalis*, *Lippia citriodora*, *Pelargonium graveolens*, and *Punica granatum*

[17]; *Prosopis cineraria* [18]; *Nigella sativa* [19]; *Jasminum auriculatum* [20]; *Avicennia marina* [21]; *Phyllanthus urinaria*, *Pouzolzia zeylanica*, and *Scoparia dulcis* [22]; *Geranium* [23]; and *Salvia officinalis* [24] were used for the synthesis of MNPs. Therein, phenolic compounds, polysaccharides, alkaloids, amino acids, terpenoids, flavonoids, and proteins presented in plant extracts demonstrated effectiveness in reducing metal ions to form MNPs with the tunable shape and size [25, 26]. The shape of the obtained nanoparticles is quite diverse, including spherical, prism, triangular, hexagonal, oval, and cubic, with a size range from 2 to 100 nm. Among the above-mentioned phytochemicals, phenolic compounds were reported as a major reducing agent in the biosynthesis of MNPs [27]. Therein, electrons generated from the phenolic groups play an important role in transforming metal ions into respective metal nanoparticles. Subsequently, phenolic groups were converted into phenoxyl radicals and then to quinones [28].

One of the most important criteria for the selection of a suitable plant is that the plant (i) should be friendly to people, (ii) should have potential biomolecule classes acting as effective stabilizing agents for preventing the agglomeration of the formed MNPs, and (iii) should not affect the properties of MNPs by masking their surface [2, 29]. Furthermore, plant sources containing phytochemicals of known nature are advised as better precursors for the MNP synthesis than an unknown [13]. In this context, *Limnophila rugosa* (Roth) Merr. (denoted by LR) is an erect herb in the genus *Limnophila* belonging to family Plantaginaceae. The plant is easy to find at low altitudes in open humid places and is used commonly as one kind of salad in many Asian countries, including Malaya, Polynesia, India, China, and Vietnam. The plant can reach a height of about 50 cm. Its leaves are in an oblong-ovate shape with a length of about 3 to 10 cm and a width of 1.5 to 4 cm, toothed at the margins [30]. The leaves themselves are the main ingredient in many traditional herbal remedies for treating various diseases, including diarrhoea, dysentery pestilent fever, and dyspepsia. Various phytochemicals from LR, such as polyphenolic compounds, flavonoids, terpenoids, amino acids, and carboxylic compounds, are very suitable for the application in the synthesis and stabilizing MNPs [31].

Nitrobenzene and nitrophenol derivatives are important manufactured chemical classes used mainly as an intermediate for producing dyestuffs, pigments, paint coloring, rubber chemicals, and fungicides [32]. Small amounts are utilized as laboratory reagents and intermediate to make drugs. The U.S. projected demand for nitrobenzene and nitrophenol derivatives is in the tens of millions of pounds a year. A small amount of those compounds discharged into the water environment is considered to be highly toxic to aquatic life with long-term hazard. For people, exposure to nitrophenols can cause headache, nausea, drowsiness, and irritation with the eyes [33]. The traditional method to handle wastewater containing nitrobenzene and nitrophenol derivatives was biological treatment combined with adsorption using powdered activated carbon and activated sludge [34]. However, the key drawback of this method is it is time consuming and ineffective compared to other advanced methods such as redox methods for converting nitrophenols to respective environmentally friendly compounds. In this context, sodium borohydride ($NaBH_4$) is widely used as an effective reducing agent for that purpose. As reported early by Kariuki et al. that $NaBH_4$ had low reduced power for nitrophenols, therein the compounds remained unchanged up to 60 min in the absence of a catalyst [29]. The reaction between nitrophenols and $NaBH_4$ can occur significantly faster in the presence of AgNPs and AuNPs as catalysts. Therefore, in the present study, a single-step method for the green synthesis of AgNPs and AuNPs using the aqueous leaf extract of LR (LR-AgNPs and LR-AuNPs, respectively) as reducing and stabilizing agents was designed. To the best of our knowledge, this is the first time LR has been used in the biosynthesis of MNPs for catalytic application. The catalytic efficiency of LR-AgNPs and LR-AuNPs in the reduction of 1,4-dinitrobenzene (1,4-DNB), 2-nitrophenol (2-NP), 3-nitrophenol (3-NP), and 4-nitrophenol (4-NP) by $NaBH_4$ was evaluated in detail.

2. Materials and Methods

2.1. Chemicals and Materials. Silver nitrate ($AgNO_3$, ≥99.8%) of reagent grade was purchased from Merck (Germany). Tetrachloroauric acid trihydrate ($HAuCl_4{\cdot}3H_2O$, ≥49.0% Au) was of ACS reagent grade supplied by Acros Organics (Belgium). Sodium tetrahydridoborate ($NaBH_4$, 99.0%), 1,4-dinitrobenzene (1,4-DNB, $C_6H_4N_2O_4$, 98.0%), and three isomers of nitrophenols, including 2-nitrophenol (2-NP, $C_6H_5NO_3$, ≥ 99%), 3-nitrophenol (3-NP, $C_6H_5NO_3$, ≥ 99%), and 4-nitrophenol (4-NP, $C_6H_5NO_3$, ≥ 99%) were commercial products from Sigma-Aldrich. All the glassware was rinsed thoroughly with deionized water and dried up before use in experiments to avoid any coagulation caused by electrolytes. Fresh LR leaves were picked in the neighbourhood of Ho Chi Minh City (Vietnam) in March 2020.

2.2. Preparation of LR Leaf Extract. Fresh LR leaves were washed many times by tap water to remove all the dirt and then rinsed thoroughly by distilled water before preparing the extract. The fresh LR leaves (5 g) were firstly mashed by a porcelain pestle and then heated in 300 mL of distilled water at 90°C with reflux for 1 h. The mixture was cooled down to room temperature. The aqueous extract of LR leaves was obtained by filtered the mixture with Whatman filter paper No.1. The freshly prepared extract was used for all experiments.

2.3. Fabrication of MNPs. The synthesis of biogenic LR-AgNPs and LR-AuNPs was performed only with the freshly prepared LR extract with $AgNO_3$ and $HAuCl_4$ solutions without using any other chemicals. In a typical procedure, 1 mL of the extract was mixed with 1 mL aqueous solution of metallic ions under vigorous stirring in the dark to avoid photochemical reactions affecting the quality of MNPs. The change in color of the solution caused by the surface plasmon resonance phenomenon (SPR) was recorded to monitor the formation of MNPs. The optimization process was performed to obtain the nanoparticles with the best size and morphology, as similarly described in our previous works [35, 36]. Three main factors, including reaction time, metallic

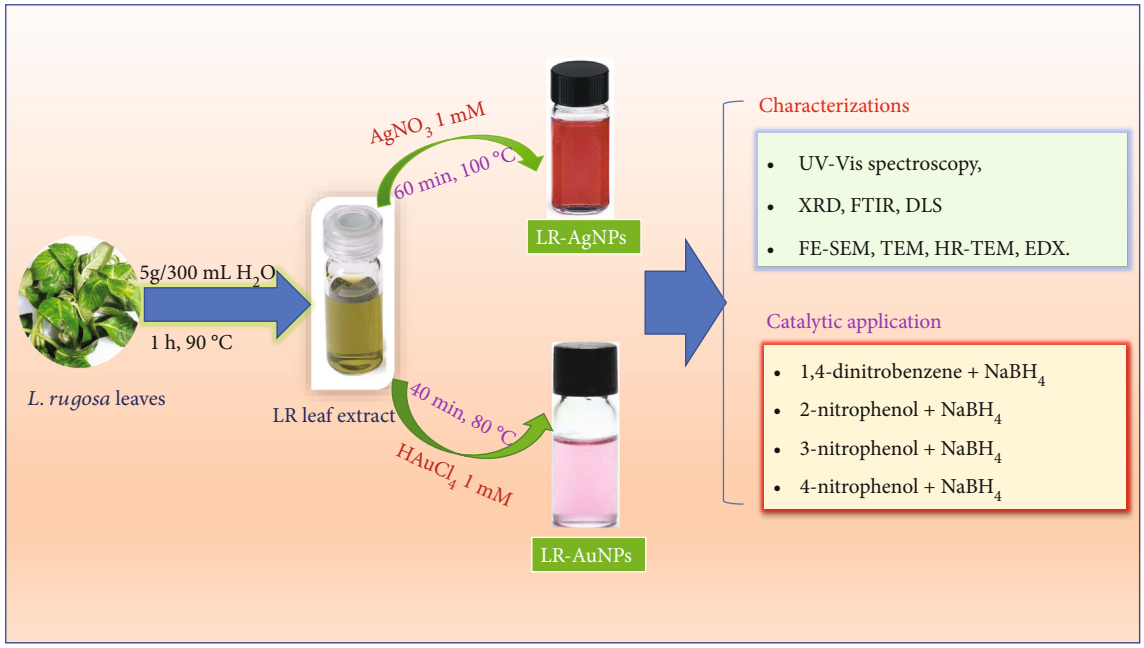


Figure 1: Biosynthesis of LR-AgNPs and LR-AuNPs with their application.

ion concentration, and reaction temperature, were investigated to determine the optimal conditions (Figure SI 1). The UV-Vis measurements were performed to find out the characteristic SPR absorbance of LR-AgNPs and LR-AuNPs at around 425 nm and 540 nm, respectively [36, 37]. The optimal conditions were chosen to be 1.0 mM, 60 min, and 100°C for the synthesis of LR-AgNPs and 1.0 mM, 40 min, and 80°C for LR-AuNPs. The MNPs biosynthesized at optimal conditions were centrifuged at 8000 rpm for 15 min, washed twice with distilled water and one time with ethanol and then dried up at 90°C overnight before characterizing their physicochemical properties. The single-step biosynthesis procedure of LR-AgNPs and LR-AuNPs using freshly prepared LR extract is illustrated in Figure 1.

2.4. Catalyst Characterization. The possible functional groups presented in the dried extract from LR leaves and fabricated solid MNPs were determined by Fourier transform infrared (FTIR) spectra recorded on a Bruker Tensor 27 (Germany) in the range of 4000-500 cm^{-1}. The crystalline nature of MNPs was examined by powder X-ray diffraction (XRD) on a 6100 X-ray diffractometer (Shimadzu, Japan) and selected area electron diffraction (SAED) patterns equipped on a high-resolution transmission electron microscopy (HR-TEM, JEM-2100, JEOL). The morphology of the nanoparticles in the colloidal solution was determined by the above-mentioned HR-TEM set at 200 kV. The determination of morphology of powdered MNPs was also performed by field-emission scanning electron microscopy (FE-SEM) on a Hitachi S-4800 HI-9057-0006 (Hitachi, Japan). The chemical elemental composition of MNPs was analyzed by energy-dispersive X-ray (EDX) spectroscopy integrated on the FE-SEM. Specimen preparation for FE-SEM/EDX analysis was as follows. The solid MNPs (1.0 mg) were dispersed in ethanol (1.0 mL) and stirred for 5 min using a glass rod. The suspension (100 μL) was dripped onto a clean carbon conductive tape premounted on aluminum stubs and then allowed to dry. In the EDX analysis, the number of iterations was set to three in different positions. The percentage of elements presented in the samples provided along with EDX spectra was the average values. The hydrodynamic particle diameter of MNPs was examined using the dynamic light scattering (DLS) technique on a Horiba SZ-100 (Japan) operated at 25°C, dispersion medium viscosity 0.896 mPa·s, and scattering angle of 90°. The UV-Vis measurements were carried out on a Metash UV-5100 UV-Vis spectrophotometer in the range of 300 to 700 nm.

2.5. Catalytic Activity Evaluation. The catalytic activity of LR-AgNPs and LR-AuNPs was evaluated toward the reduction of 1,4-DNB and three isomers of nitrophenols (2-NP, 3-NP, and 4-NP) using an excess amount of $NaBH_4$ at ambient temperature. Briefly, 2.5 mL 1.0 mM of each pollutant and 0.5 mL 0.1 M of $NaBH_4$ were mixed in a quartz cuvette with an optical path length of 10 mm, and then, 3 mg of MNPs was added. The UV-Vis spectra at the wavelength ranged from 250 to 600 nm were recorded over time t. To study the kinetics of this pseudo-first-order reaction, a linear regression of $\ln(A_t)$ over reaction time t was plotted. The reaction rate constant k was determined from the slope of the straight line $\ln(A_t) = f(t)$ [35]. In a reusability study of MNPs, the catalysts were centrifuged and washed twice with distilled water and twice with ethanol before reuse.

3. Results and Discussions

3.1. Characterization of MNPs. The FTIR spectroscopy is usually used for proving the presence of functional groups of biomolecules in the extract that acted as reducing and capping agents. Figure 2(a) showed the FTIR spectra of the dried extract from LR leaves and LR-capped MNPs. Accordingly,

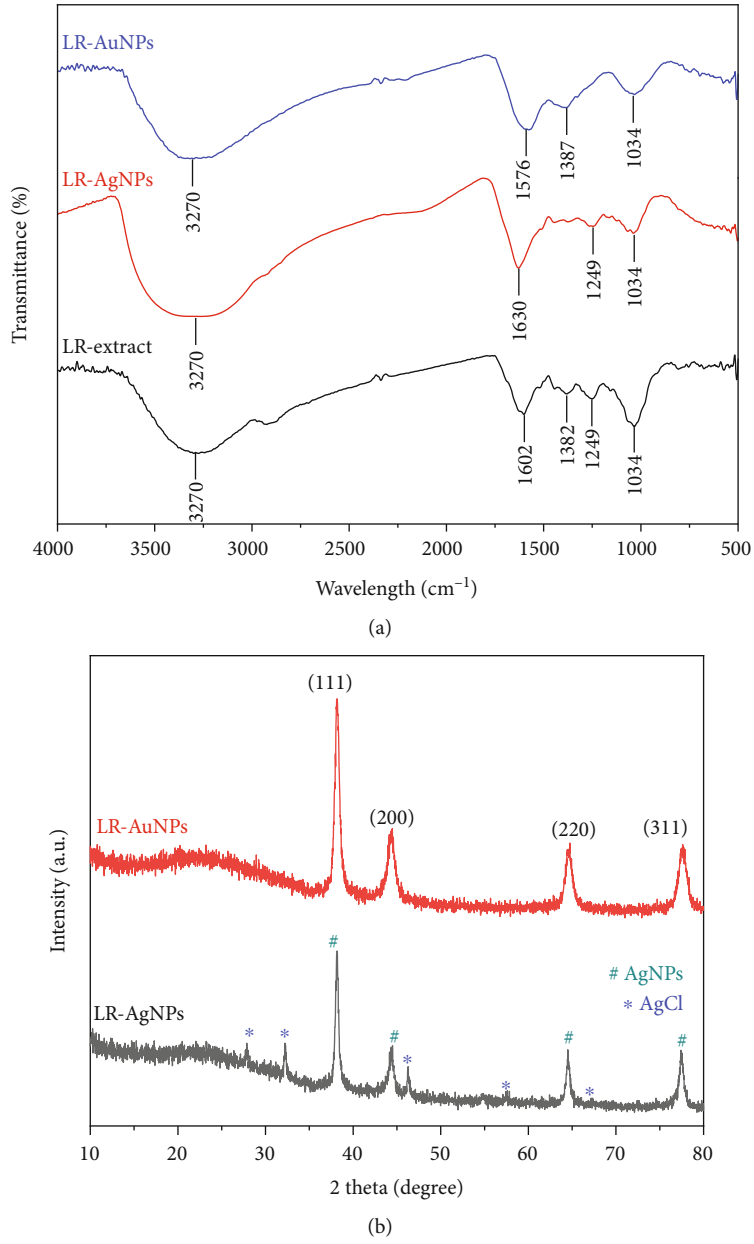


Figure 2: FITR spectra (a) and XRD patterns (b) of LR-AgNPs and LR-AuNPs.

the FTIR spectrum of the dried extract and biosynthesized MNPs showed that almost no difference in the number of characteristic peaks and their intensity for all sample was observed. The major bands of the LR extract were recorded at 3270, 1602, 1382, 1249, and 1034 cm^{-1}. The broad band at 3270 cm^{-1} is attributed to the stretching vibration of hydroxyl groups in polyphenolic compounds, terpenoids containing alcohol functional groups, and carboxylic compounds presented in the LR leaves extract as mentioned before [21, 38]. The high-intensity peak at 1602 cm^{-1} is associated with C=C and C=O vibrations of benzene rings and carbonyl groups of amino acids [39]. The peak at 1382 cm^{-1} is assigned to stretching vibrations of the carboxylate groups [40]. The absorption band at 1249 cm^{-1} is related to hydroxyl groups in polyphenolic compounds with the in-plane bending vibration [41]. The peak at 1034 cm^{-1} is identified with C–O band stretching of flavonoids [42]. The small shift of several bands can be due to interaction between functional groups of biomolecules and nanoparticles. It should be noted that the peak at 1382 cm^{-1} in the FTIR spectrum of LR-AgNPs was strongly reduced. Accordingly, respective polyphenolic groups are proven as the main reducing agents in the biosynthesis of MNPs. Along with this fact, other functional groups in biomolecules presented in the extract are also confirmed for the stabilization of MNPs.

The crystalline phase composition and crystal size of LR-AgNPs and LR-AuNPs were examined by XRD patterns, as shown in Figure 2(b). The XRD pattern of LR-AuNPs shows Bragg reflections of pure gold metal at 2θ values of 38.2°, 44.4°, 64.7°, and 77.5°. According to the ICDD PDF card

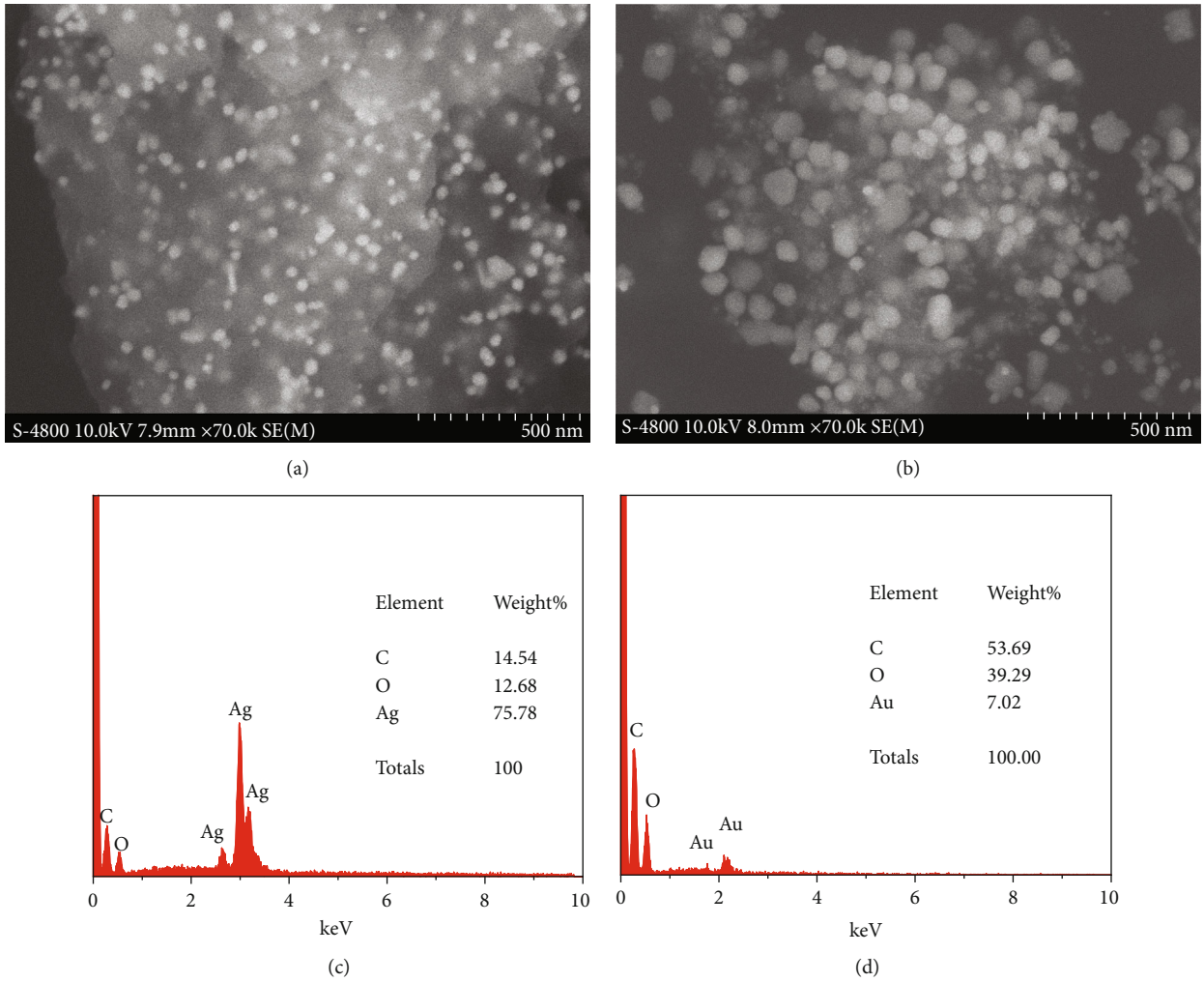


Figure 3: FE-SEM images and EDX spectra of LR-AgNPs (a, c) and LR-AuNPs (b, d).

no. 00-004-0784, the biosynthesized LR-AuNPs possess the face-centered cubic (FCC) structure with four main lattice planes indexed as (111), (200), (220), and (311). In the case of LR-AgNPs, the Bragg reflections were observed at 28.5°, 32.3°, 38.2°, 45.6°, 46.3°, 66.5°, and 77.5°. Herein, the high-intensity peaks at 38.2°, 45.6°, 66.5°, and 77.5° generated from (111), (200), (220), and (311) planes, respectively, are related to the FCC structure of silver metal, which is confirmed by the card no. 00-004-0783. The low-intensity peaks at 28.5°, 32.3°, and 46.3° are identified with crystalline AgCl according to the card no. 00-001-1013. The presence of a small amount of AgCl along with silver in the LR-AgNP sample can be due to the reaction between Ag^+ and a little amount of Cl^- presented in LR leaf extract. Many previous works also reported similar results on AgCl composition in AgNPs biosynthesized using aqueous leaf extract as reducing agents [39, 43].

The XRD patterns of the biosynthesized MNPs were also utilized to calculate their nanocrystallite size based on the Monshi–Scherrer equation as below [44, 45]. The Monshi–Scherrer equation (Equation (1)) is the modified Scherrer equation recently advised to estimate more accurately nanocrystallite size using XRD:

$$\mathrm{Ln}\beta = \mathrm{Ln}\left(\frac{K\lambda}{L}\right) + \mathrm{Ln}\left(\frac{1}{\cos\theta}\right), \quad (1)$$

where β is the full width at half maximum in radians, $K = 0.9$ is the Scherrer constant usually used for spherical crystals, $\lambda = 0.1504$ nm is the wavelength of the X-ray, L is the average crystallite size in nm, and θ is the reflected Bragg angle. By plotting $\mathrm{Ln}\beta$ versus $\mathrm{Ln}(1/cos\theta)$, the value of $\mathrm{Ln}(K\lambda/L)$ can be determined from the intercept, followed by the average crystallite size L. Accordingly, the average crystallite size of LR-AgNPs and LR-AuNPs is estimated to be about 25.3 nm and 22.9 nm, respectively. Meanwhile, the average crystallite size of AgCl calculated based on the Monshi–Scherrer equation is about 38.1 nm.

The surface morphology and elemental composition of the biosynthesized MNPs are determined by SEM and EDX analysis, as presented in Figure 3. The SEM images of biosynthesized LR-AgNPs (Figure 3(a)) and LR-AuNPs (Figure 3(b)) reveal that both MNPs have mostly spherical shapes dispersed nonuniformly and tend to form clusters, especially for LR-AuNPs. The EDX spectra (Figures 3(c) and 3(d)) show that the

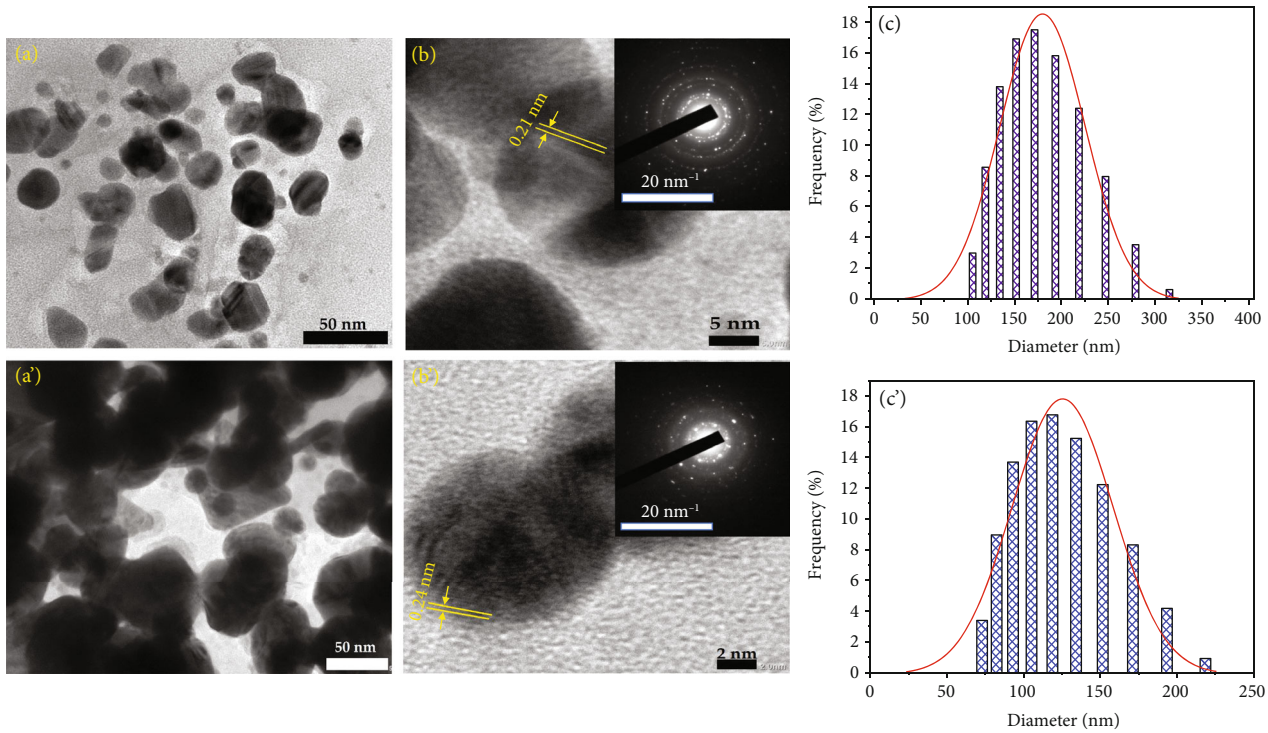


Figure 4: TEM images (a, a'), HR-TEM and SEAD images (b, b'), and DLS (c, c') of LR-AgNPs (a, b, c) and LR-AuNPs (a', b', c').

biosynthesized MNPs consist mainly of metal elements (Ag or Au), carbon, and oxygen. A large amount of silver (75.78%) in LR-AgNPs was verified by strong characteristic peaks at 2.65, 2.85, and 2.95 keV. The presence of carbon (14.54%) and oxygen (12.68%) confirmed the respective peaks at 0.255 and 0.53 keV. For LR-AuNPs, gold metal (7.02%) appeared with characteristic peaks at 1.74 and 2.195 keV; meanwhile, carbon (53.69%) and oxygen (39.29%) were also observed at 0.255 and 0.53 keV, respectively (Figure 3(d)). It is worth noting that the large amount of carbon detected in LR-AuNPs could be partly due to using a carbon conductive tape in the specimen preparation. Nevertheless, the gold content is still lower than the silver element; in contrast, the total content of carbon and oxygen in LR-AuNPs is far beyond LR-AgNPs. The reason can be that gold ions with the positive charge of 3+ can attract more organic molecules in LR leaf extract than Ag^{+}.

The shape, size, and crystalline nature of MNPs were confirmed by TEM analysis. Figures 4(a) and 4(a') show the TEM images of LR-AgNPs and LR-AuNPs, respectively. It is evident from the TEM images that the LR-MNPs are nearly in a spherical shape and link together to form clusters. A thin layer of biomolecules acting as a capping agent was also observed, which is probably the reason for the cluster formation. A cross-linking between surrounding biomolecules of two or more nanoparticles can be formed via hydrogen bonds due to the presence of many acidic/basic functional groups such as amine, alcohol, and carboxylic groups [1]. The TEM images of LR-MNPs show that the nanoparticles come in many different sizes. The HR-TEM images of LR-AgNPs and LR-AuNPs indicate that their lattice fringes are 0.21 nm and 0.24 nm, respectively, which is in a good correlation with the d-spacing between (111) reflection planes in the metals' FCC structure given by XRD data. The SAED patterns (inserts in Figures 4(b) and 4(b')) also show bright rings, confirming the crystalline nature of the biosynthesized MNPs. Furthermore, the radius of the ring assigned to (111) planes from the SAED data was calculated to be 4.76 nm for LR-AgNPs and 4.17 nm for LR-AuNPs. According to the formula of d − spacing = $1/r$, where r is the radius of the ring, the established d-spacing values between (111) planes of LR-AgNPs and LR-AuNPs were consistent with those of XRD data and HR-TEM images. The mean size of nanoparticles is found to be 87.5 nm for LR-AgNPs and 122.8 nm for LR-AuNPs according to particle size distribution diagrams obtained by the DLS method (Figures 4(c) and 4(c')).

3.2. Catalytic Activity of MNPs. In the present work, the catalytic performance of the biosynthesized MNPs was evaluated based on the reduction of 1,4-DNB, 2-NP, 3-NP, and 4-NP by $NaBH_4$ into the respective useful nontoxic aminophenols. This reaction without catalyst was recognized as unfavorable because of a large energy activation caused by the kinetic barrier between the BH_4^- and nitrophenolate ions [35]. In the presence of MNPs, a new route of electron transfer from BH_4^- to nitrophenolate ions via the catalyst surface was established, leading to the decrease in energy activation of the reaction. As reported in previous works, the kinetics of the reaction between nitrophenols and $NaBH_4$ using MNPs as a catalyst can be described by the Langmuir-Hinshelwood model with a 3-stage mechanism [46, 47]. In the first stage, a rapid reversible adsorption of both nitrophenolate ions and BH_4^- on the surface of MNPs was established. Because the catalytic

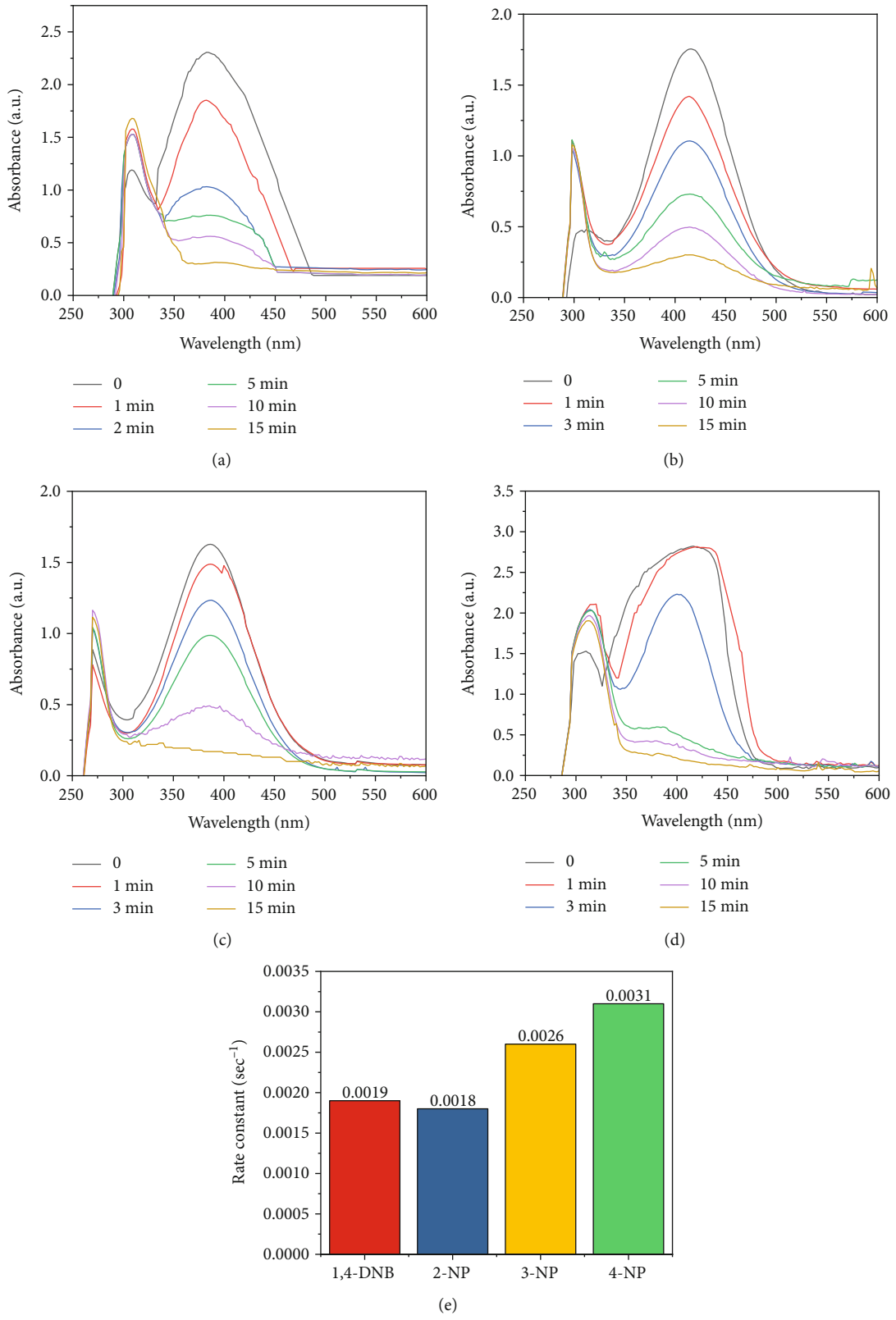


Figure 5: Reduction of 1,4-DNB (a), 2-NP (b), 3-NP (c), and 4-NP (d) by LR-AgNPs and first-order reduction rate constants (e).

reduction proceeded on the heterogenous catalyst surface, the concentration of adsorbed reactants will decide the reaction rate. In the second stage, electrons transported from BH_4^- to nitro groups of nitrophenolate ions through active sites of MNPs, followed by the formation of respective aminophenols. The third stage started when the concentration of products

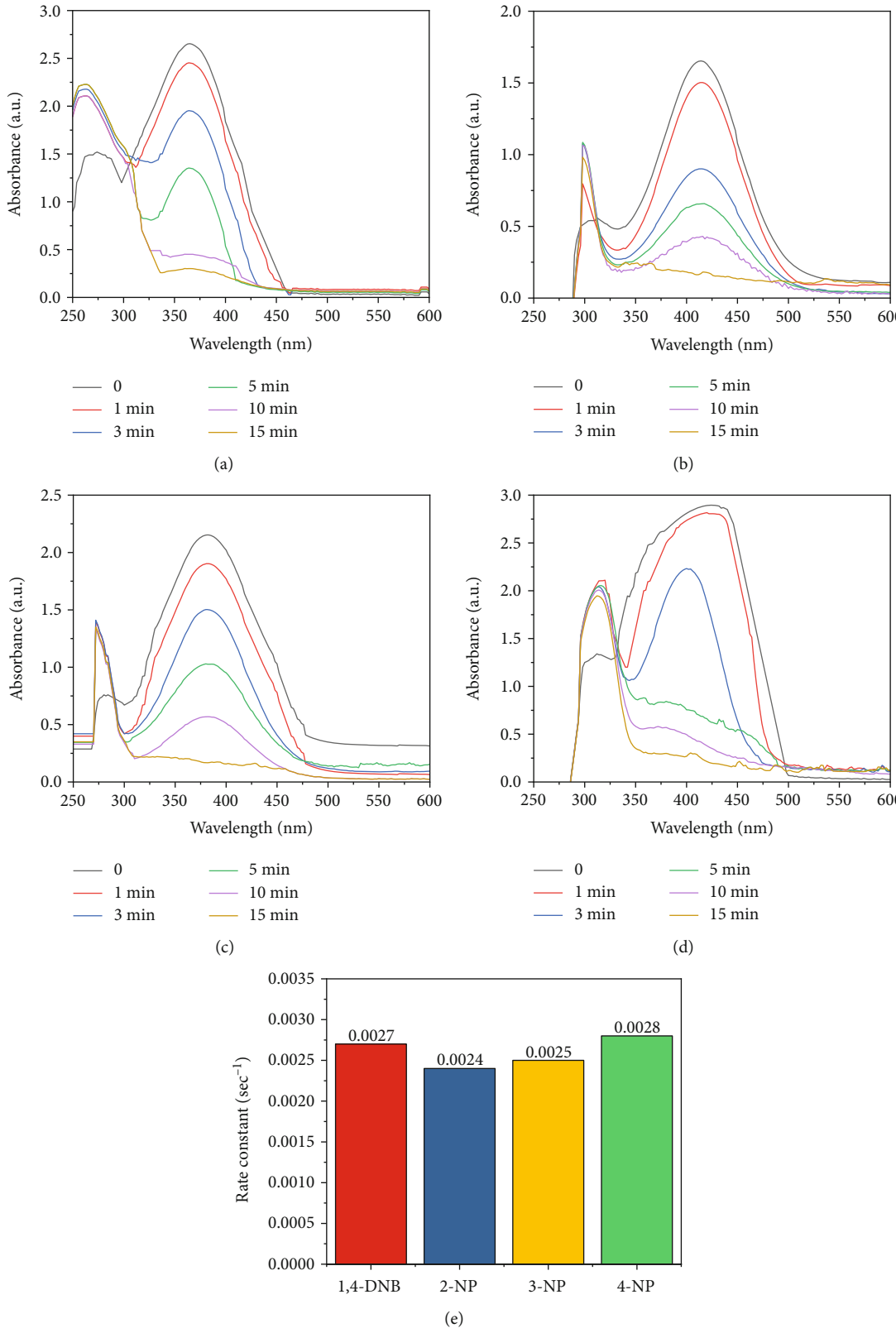


Figure 6: Reduction of 1,4-DNB (a), 2-NP (b), 3-NP (c), and 4-NP (d) by LR-AuNPs and first-order reduction rate constants (e).

was high enough, they were released from the catalyst surface, and vacant active sites on the catalyst surface resumed a new cycle of the reduction.

Figures 5 and 6 show the degradation of nitrophenols in the presence of the biosynthesized MNPs and the comparison between their reaction rate constants. After the addition

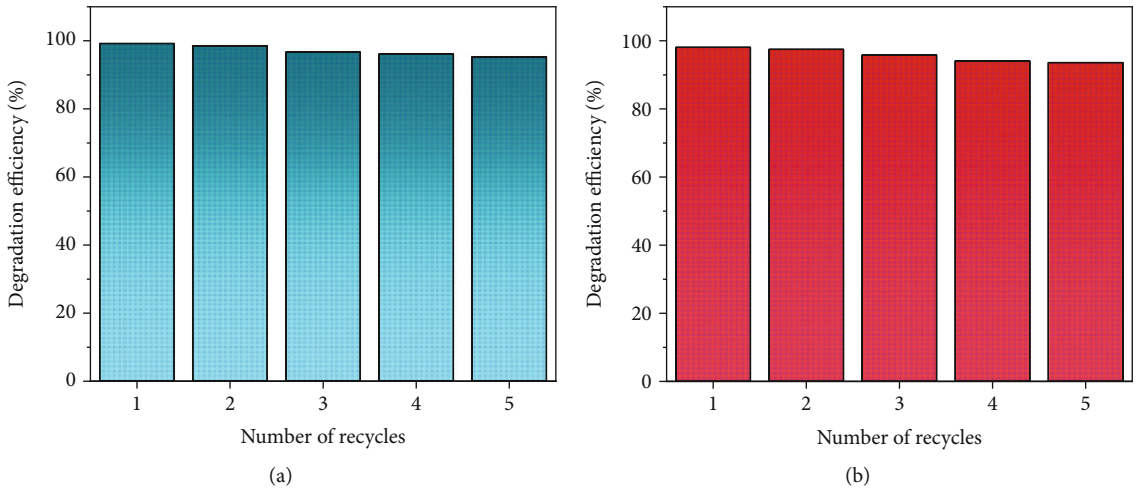


Figure 7: Reusability of LR-AgNPs (a) and LR-AuNPs (b) for reduction of 4-NP.

of $NaBH_4$, 1,4-DNB, 2-NP, 3-NP, and 4-NP have maximum absorbance at 380, 415, 391, and 400 nm, respectively. Upon completing the catalyst addition, the reaction took place, resulting in a decrease of nitrophenolate concentration, and the regular decline of the corresponding peaks was observed. In this study, the amount of $NaBH_4$ was designed to exceed the concentration of nitrophenols and was considered unchanged over time. The reduction was supposed as a pseudo-first-order reaction whose rate depends mainly on nitrophenol concentration and can be described by the linear equation $\ln(A_t) = -kt + \ln(A_o)$. As shown in Figures 5(a)–5(d) and 6(a)–6(d), the reduction with LR-AgNPs and LR-AuNPs was almost completed in 15 min for all nitrophenols. For LR-AgNPs, the reaction rate constants of 1,4-DNB, 2-NP, 3-NP, and 4-NP increased slightly, which were calculated to be 1.9×10^{-3}, 1.8×10^{-3}, 2.6×10^{-3}, and $3.1 \times 10^{-3}\ s^{-1}$, respectively. In the case of LR-AuNPs, a slight difference in the reaction rate constants of those pollutants was also observed, estimated to be 2.7×10^{-3}, 2.4×10^{-3}, 2.5×10^{-3}, and $2.8 \times 10^{-3}\ s^{-1}$, respectively. It is noticeable that the slight increase in reaction rate constants in order from 2-NP to 4-NP was observed for both LR-AgNPs and LR-AuNPs. The rank of the catalytic activity can be correlated to the structure of each nitrophenol compound. As mentioned before, the reduction reaction took place only after contact between $NaBH_4$ and the nitro group of nitrophenolate was established on the catalyst surface. Therefore, phenolic groups in the ortho- and meta positions may cause a little space effect, hindering this exposure. The presence of AgCl in LR-AgNPs may positively affect its catalytic activity in the first use [39]. However, a comparison of XRD intensity showed that there was only small amount of AgCl; therefore, this influence is considered as not very significant and may be negligible. The LR-AgNP and LR-AuNP samples demonstrated a quite good catalyst performance compared to those of some MNPs synthesized by the extract from various plants [34, 43].

3.3. Reusability. In this study, the long-term use of LR-AgNPs and LR-AuNPs was examined for further application in practice to effectively reduce the cost. The catalytic activity of the catalysts was reassessed in five reaction cycles. After each reuse, the catalyst was washed with distilled water and then ethanol several times. Figures 7(a) and 7(b) show the respective recyclable catalytic performance of the biosynthesized LR-AgNPs and LR-AuNPs towards 4-NP as a representative for nitrophenols. The recycling process revealed that the catalytic performance was almost unchanged, only a slight decrease was observed after the fifth recycle run with the reduction efficiency greater than 96% for CP-AuNPs and 93% for CP-AuNPs. The negligible decrease in the catalytic efficiency may be related to the loss of material during recovery.

4. Conclusions

In summary, a simple green synthesis of silver and gold nanoparticles has been successfully implemented by using the extract from *Limnophila rugosa* leaves as an effective reducing agent and capping agent. This method not only offered a cost-effective, eco-friendly, and nontoxic green route but also confirmed the possibility of using vegetables as abundant plant sources for the synthesis of noble metal nanoparticles. The synthesized LR-AgNPs and LR-AuNPs exhibited an excellent catalytic performance toward several nitrophenol derivatives using $NaBH_4$ as reductant. Besides, the produced MNPs also showed high reusability with a reduction efficiency greater than 93% after five repeated reuses. Therefore, it can reasonably be expected that the successful preparation of LR-AgNPs and LR-AuNPs would strengthen the catalytic application of novel metal nanoparticles.

Data Availability

The data used to support the findings of this study are included within the article.

Conflicts of Interest

The authors report no conflicts of interest.

Supplementary Materials

Figure SI 1: UV-Vis spectra of LR-AgNPs (above) and LR-AuNPs (bellow): concentration (a and a'), reaction time (b and b'), and reaction temperature (c and c'). *(Supplementary Materials)*

References

[1] B. Laban, U. Ralević, S. Petrović et al., "Green synthesis and characterization of nontoxic L-methionine capped silver and gold nanoparticles," *Journal of Inorganic Biochemistry*, vol. 204, p. 110958, 2020.

[2] N. Cyril, J. B. George, P. V. Nair et al., "Catalytic activity of *Derris trifoliata* stabilized gold and silver nanoparticles in the reduction of isomers of nitrophenol and azo violet," *Nano-Structures and Nano-Objects*, vol. 22, p. 100430, 2020.

[3] K. Shrivas, A. Ghosale, P. K. Bajpai, T. Kant, K. Dewangan, and R. Shankar, "Advances in flexible electronics and electrochemical sensors using conducting nanomaterials: a review," *Microchemical Journal*, vol. 156, p. 104944, 2020.

[4] F. Behzad, S. M. Naghib, M. A. J. Kouhbanani, S. N. Tabatabaei, Y. Zare, and K. Y. Rhee, "An overview of the plant-mediated green synthesis of noble metal nanoparticles for antibacterial applications," *Journal of Industrial and Engineering Chemistry*, vol. 94, pp. 92–104, 2021.

[5] C. G. A. Das, V. G. Kumar, T. S. Dhas et al., "Antibacterial activity of silver nanoparticles (biosynthesis): a short review on recent advances," *Biocatalysis and Agricultural Biotechnology*, vol. 27, p. 101593, 2020.

[6] J. Gubitosa, V. Rizzi, P. Fini et al., "Multifunctional green synthetized gold nanoparticles/chitosan/ellagic acid self-assembly: antioxidant, sun filter and tyrosinase-inhibitor properties," *Materials Science and Engineering: C*, vol. 106, p. 110170, 2020.

[7] D. C. Luther, R. Huang, T. Jeon et al., "Delivery of drugs, proteins, and nucleic acids using inorganic nanoparticles," *Advanced Drug Delivery Reviews*, vol. 156, pp. 188–213, 2020.

[8] S. Lee and B.-H. Jun, "Silver nanoparticles: synthesis and application for nanomedicine," *International Journal of Molecular Sciences*, vol. 20, no. 4, p. 865, 2019.

[9] B. P. Upoma, F. Mahnaz, W. Rahman Sajal, N. Zahan, M. S. Hossain Firoz, and M. S. Azam, "Bio-inspired immobilization of silver and gold on magnetic graphene oxide for rapid catalysis and recyclability," *Journal of Environmental Chemical Engineering*, vol. 8, no. 3, article 103739, 2020.

[10] N. Garg, S. Bera, L. Rastogi, A. Ballal, and M. V. Balaramakrishna, "Synthesis and characterization of L-asparagine stabilised gold nanoparticles: catalyst for degradation of organic dyes," *Spectrochimica Acta Part A: Molecular and Biomolecular Spectroscopy*, vol. 232, article 118126, 2020.

[11] C. Daruich De Souza, B. Ribeiro Nogueira, and M. E. C. M. Rostelato, "Review of the methodologies used in the synthesis gold nanoparticles by chemical reduction," *Journal of Alloys and Compounds*, vol. 798, pp. 714–740, 2019.

[12] O. Pryshchepa, P. Pomastowski, and B. Buszewski, "Silver nanoparticles: synthesis, investigation techniques, and properties," *Advances in Colloid and Interface Science*, vol. 284, article 102246, 2020.

[13] S. Iravani, H. Korbekandi, S. V. Mirmohammadi, and B. Zolfaghari, "Synthesis of silver nanoparticles: chemical, physical and biological methods," *Research in Pharmaceutical Sciences*, vol. 9, no. 6, pp. 385–406, 2014.

[14] K. S. Siddiqi, A. Husen, and R. A. K. Rao, "A review on biosynthesis of silver nanoparticles and their biocidal properties," *Journal of Nanobiotechnology*, vol. 16, no. 1, p. 14, 2018.

[15] M. Zhou, J. Yin, X. Zhao et al., "Green synthesis of gold nanoparticles using *Sargassum carpophyllum* extract and its application in visual detection of melamine," *Colloids and Surfaces A: Physicochemical and Engineering Aspects*, vol. 603, article 125293, 2020.

[16] J. L. Gardea-Torresdey, E. Gomez, J. R. Peralta-Videa, J. G. Parsons, H. Troiani, and M. Jose-Yacaman, "Alfalfa sprouts: a natural source for the synthesis of silver nanoparticles," *Langmuir*, vol. 19, no. 4, pp. 1357–1361, 2003.

[17] Y. Zeiri, P. Elia, R. Zach, S. Hazan, S. Kolusheva, and Z.'. Porat, "Green synthesis of gold nanoparticles using plant extracts as reducing agents," *International Journal of Nanomedicine*, vol. 9, pp. 4007–4021, 2014.

[18] Y. Periyasamy, B. Baskaran, V. Senniappan, and S. Chidambaram, "Green synthesis and characterization of silver nanomaterials using leaf extract of Prosopis cineraria for antibacterial and anti-cancer applications," *Materials Research Express*, vol. 5, no. 10, article 105402, 2018.

[19] K. Chand, C. Jiao, M. N. Lakhan et al., "Green synthesis, characterization and photocatalytic activity of silver nanoparticles synthesized with *Nigella sativa* seed extract," *Chemical Physics Letters*, vol. 763, article 138218, 2021.

[20] S. Balasubramanian, S. M. J. Kala, and T. L. Pushparaj, "Biogenic synthesis of gold nanoparticles using *Jasminum auriculatum* leaf extract and their catalytic, antimicrobial and anticancer activities," *Journal of Drug Delivery Science and Technology*, vol. 57, p. 101620, 2020.

[21] K. S. B. Naidu, N. Murugan, J. K. Adam, and Sershen, "Biogenic synthesis of silver nanoparticles from *Avicennia marina* seed extract and its antibacterial potential," *Bionanoscience*, vol. 9, no. 2, pp. 266–273, 2019.

[22] D. H. Nguyen, J. S. Lee, K. D. Park et al., "Green silver nanoparticles formed by Phyllanthus urinaria, Pouzolzia zeylanica, and Scoparia dulcis leaf extracts and the antifungal activity," *Nanomaterials*, vol. 10, no. 3, p. 542, 2020.

[23] R. D. Rivera-Rangel, M. P. González-Muñoz, M. Avila-Rodriguez, T. A. Razo-Lazcano, and C. Solans, "Green synthesis of silver nanoparticles in oil-in-water microemulsion and nanoemulsion using geranium leaf aqueous extract as a reducing agent," *Colloids and Surfaces A: Physicochemical and Engineering Aspects*, vol. 536, pp. 60–67, 2018.

[24] R. Ghahremanzadeh, F. Yazdi Samadi, and M. Yousefi, "Green synthesis of gold nanoparticles using three medicinal plant extracts as efficient reducing agents," *Iranian Journal of Chemistry and Chemical Engineering*, vol. 38, no. 1, pp. 1–10, 2014.

[25] S. S. Sana and L. K. Dogiparthi, "Green synthesis of silver nanoparticles using Givotia moluccana leaf extract and evaluation of their antimicrobial activity," *Materials Letters*, vol. 226, pp. 47–51, 2018.

[26] T.-T. Vo, T. T.-N. Nguyen, T. T.-T. Huynh et al., "Biosynthesis of silver and gold nanoparticles using aqueous extract from *Crinum latifolium* leaf and their applications forward antibacterial effect and wastewater treatment," *Journal of Nanomaterials*, vol. 2019, 14 pages, 2019.

[27] A. M. El Shafey, "Green synthesis of metal and metal oxide nanoparticles from plant leaf extracts and their applications:

a review," *Green Processing and Synthesis*, vol. 9, no. 1, pp. 304–339, 2020.

[28] J. A. Jacob, H. S. Mahal, N. Biswas, T. Mukherjee, and S. Kapoor, "Role of phenol derivatives in the formation of silver nanoparticles," *Langmuir*, vol. 24, no. 2, pp. 528–533, 2008.

[29] V. M. Kariuki, I. Yazgan, A. Akgul, A. Kowal, M. Parlinska, and O. A. Sadik, "Synthesis and catalytic, antimicrobial and cytotoxicity evaluation of gold and silver nanoparticles using biodegradable, *Π*-conjugated polyamic acid," *Environmental Science. Nano*, vol. 2, no. 5, pp. 518–527, 2015.

[30] K. S. Mukherjee, D. Gorai, S. M. A. Sohel et al., "*A new flavonoid from Limnophila rugosa*," *Fitoterapia*, vol. 74, no. 1-2, pp. 188–190, 2003.

[31] S. M. D. Gorai, S. K. Jash, R. K. Singh, and A. Sarkar, "Chemical and pharmacological aspects of *Limnophila rugosa*: an update," *International Journal of Natural Products Research*, vol. 3, pp. 120–124, 2013.

[32] P. K. Arora, A. Srivastava, and V. P. Singh, "Bacterial degradation of nitrophenols and their derivatives," *Journal of Hazardous Materials*, vol. 266, pp. 42–59, 2014.

[33] Z. Xiong, H. Zhang, W. Zhang, B. Lai, and G. Yao, "Removal of nitrophenols and their derivatives by chemical redox: a review," *Chemical Engineering Journal*, vol. 359, pp. 13–31, 2019.

[34] B. Petrova, B. Tsyntsarski, T. Budinova, N. Petrov, L. F. Velasco, and C. O. Ania, "Activated carbon from coal tar pitch and furfural for the removal of p-nitrophenol and m-aminophenol," *Chemical Engineering Journal*, vol. 172, no. 1, pp. 102–108, 2011.

[35] V.-D. Doan, A. T. Thieu, T.-D. Nguyen et al., "Biosynthesis of gold nanoparticles using *Litsea cubeba* fruit extract for catalytic reduction of 4-nitrophenol," *Journal of Nanomaterials*, vol. 2020, Article ID 4548790, 10 pages, 2020.

[36] V.-D. Doan, B.-A. Huynh, T.-D. Nguyen et al., "Biosynthesis of silver and gold nanoparticles using aqueous extract of *Codonopsis pilosula* roots for antibacterial and catalytic applications," *Journal of Nanomaterials*, vol. 2020, 18 pages, 2020.

[37] T. T. Vo, C. H. Dang, V. D. Doan, V. S. Dang, and T. D. Nguyen, "Biogenic synthesis of silver and gold nanoparticles from *Lactuca indica* leaf extract and their application in catalytic degradation of toxic compounds," *Journal of Inorganic and Organometallic Polymers and Materials*, vol. 30, no. 2, pp. 388–399, 2020.

[38] I. Sk, M. A. Khan, A. Haque et al., "Synthesis of gold and silver nanoparticles using _Malva verticillata_ leaves extract: Study of gold nanoparticles catalysed reduction of nitro-Schiff bases and antibacterial activities of silver nanoparticles," *Current Research in Green and Sustainable Chemistry*, vol. 3, p. 100006, 2020.

[39] V. D. Doan, M. T. Phung, T. L. H. Nguyen, T. C. Mai, and T. D. Nguyen, "Noble metallic nanoparticles from waste Nypa fruticans fruit husk: biosynthesis, characterization, antibacterial activity and recyclable catalysis," *Arabian Journal of Chemistry*, vol. 13, no. 10, pp. 7490–7503, 2020.

[40] S. Nayak, S. P. Sajankila, and C. V. Rao, "Green synthesis of gold nanoparticles from banana pith extract and its evaluation of antibacterial activity and catalytic reduction of malachite green dye," *Journal of Microbiology, Biotechnology and Food Sciences*, vol. 7, no. 6, pp. 641–645, 2018.

[41] M. A. Odeniyi, V. C. Okumah, B. C. Adebayo-Tayo, and O. A. Odeniyi, "Green synthesis and cream formulations of silver nanoparticles of Nauclea latifolia (African peach) fruit extracts and evaluation of antimicrobial and antioxidant activities," *Sustainable Chemistry and Pharmacy*, vol. 15, p. 100197, 2020.

[42] P. Kaithavelikkakath Francis, S. Sivadasan, A. Avarachan, and A. Gopinath, "A novel green synthesis of gold nanoparticles using seaweedLobophora variegataand its potential application in the reduction of nitrophenols," *Particulate Science and Technology*, vol. 38, no. 3, pp. 365–370, 2020.

[43] V. D. Doan, V. T. Le, T. D. Nguyen, T. L. H. Nguyen, and H. T. Nguyen, "Green synthesis of silver nanoparticles usingaganonerion polymorphumleaves extract and evaluation of their antibacterial and catalytic activity," *Materials Research Express*, vol. 6, no. 11, 2019.

[44] M. Rabiei, A. Palevicius, A. Monshi, S. Nasiri, A. Vilkauskas, and G. Janusas, "Comparing methods for calculating nano crystal size of natural hydroxyapatite using X-ray diffraction," *Nanomaterials*, vol. 10, no. 9, p. 1627, 2020.

[45] A. Monshi, M. R. Foroughi, and M. R. Monshi, "Modified Scherrer equation to estimate more accurately nanocrystallite size using XRD," *World Journal of Nano Science and Engineering*, vol. 2, no. 3, pp. 154–160, 2012.

[46] F. Torkamani and S. Azizian, "Green and simple synthesis of Ag nanoparticles loaded onto cellulosic fiber as efficient and low-cost catalyst for reduction of 4-nitrophenol," *Journal of Molecular Liquids*, vol. 214, pp. 270–275, 2016.

[47] P. Suchomel, L. Kvitek, R. Prucek et al., "Simple size-controlled synthesis of Au nanoparticles and their size-dependent catalytic activity," *Scientific Reports*, vol. 8, no. 1, p. 4589, 2018.